ADVANCED MATERIALS TECHNOLOGIES
www.advmattechnol.de

Improved Long-Term Stability and Reduced Humidity Effect in Gas Sensing: SiO_2 Ultra-Thin Layered ZnO Columnar Films

Vasile Postica, Oleg Lupan, Anna Gapeeva, Luka Hansen, Rasoul Khaledialidusti, Abhishek Kumar Mishra, Jonas Drewes, Holger Kersten, Franz Faupel, Rainer Adelung,* and Sandra Hansen*

The undoped and metal-doped zinc oxide columnar films (ZnO:Sn, ZnO:Fe, ZnO:Ag, and ZnO:Cu) are covered with an ultra-thin layer of SiO_2 (10–20 nm). The electrical, UV, and volatile organic compounds (VOCs) sensing properties are evaluated under different ambient conditions for ≈7 months to investigate the impact of the top SiO_2-layer on the long-term stability of samples. The obtained results show a high immunity of sensing properties of SiO_2-coated samples to humidity. Furthermore, gas sensing measurements show that the loss in response after 203 days is significantly lower for coated samples indicating higher stability of sensing performance. For ZnO:Fe the gas response is reduced by about 90% after 203 days, but for SiO_2-coated ZnO:Fe columnar films the gas response is slightly reduced by only 38%. The density functional theory (DFT) calculations show that water species bind strongly with the surface SiO_2 layer atoms with a –0.129 e^- charge transfer, which is, much higher compared to the interaction with ethanol and acetone. Calculations show strong binding of water species on the SiO_2 layer indicating preferential absorption of water molecules on SiO_2. The obtained results demonstrate an important role of the top SiO_2 ultra-thin layer in order to produce humidity-tolerant sensitive devices.

1. Introduction

Based on the interesting and multifunctional characteristics of ZnO, including partly covalent and partly ionic character, its nano- and microstructures have been extensively used for gas sensor applications.[1–4] However, the low selectivity and poor gas detection characteristics of sensing devices based on nano- and microstructures of metal oxides is a well-known issue.[5,6] In a humid ambient/environment, on the same sites as adsorbed O, H_2O molecules are adsorbed by conversion to the hydroxyl groups.[7] The hydroxyl poisoning can be expressed by[7]

$$H_2O + O^-(O^{2-}) + S \rightarrow 2(S-OH) + e^-(2e^-) \quad (1)$$

where S is the adsorption site on the metal oxide and e– is the electron. Thus, in a humid atmosphere, hydroxyl groups

V. Postica, Prof. O. Lupan
Center for Nanotechnology and Nanosensors
Technical University of Moldova
168 Stefan cel Mare Av., Chisinau MD-2004, Republic of Moldova
E-mail: ollu@tf.uni-kiel.de; oleg.lupan@mib.utm.md

Prof. O. Lupan, A. Gapeeva, Prof. R. Adelung, Dr. S. Hansen
Functional Nanomaterials
Institute for Materials Science
Faculty of Engineering
Kiel University
Kaiserstr. 2, D-24143 Kiel, Germany
E-mail: ra@tf.uni-kiel.de

The ORCID identification number(s) for the author(s) of this article can be found under https://doi.org/10.1002/admt.202001137.

DOI: 10.1002/admt.202001137

L. Hansen, Prof. H. Kersten
Plasma Technology
Institute of Experimental and Applied Physics
Kiel University
Leibnizstr. 19, D-24098 Kiel, Germany

Dr. R. Khaledialidusti
Department of Mechanical and Industrial Engineering
Norwegian University of Science and Technology (NTNU)
Trondheim 7491, Norway

Prof. A. K. Mishra
Department of Physics
School of Engineering
University of Petroleum and Energy Studies
Bidholi via Premnagar
Dehradun 248007, India

J. Drewes, Prof. F. Faupel
Chair for Multicomponent Materials
Institute for Materials Science
Faculty of Engineering
Kiel University
Kaiserstr. 2, D-24143 Kiel, Germany

are adsorbed and S—OH groups are formed by substitution of oxygen species while electrons are donated to oxygen.[6–8] Due to a diminishing in the oxygen coverage, the sensitivity in a humid atmosphere is reduced. Therefore, to obtain high stability of metal oxide-based sensors in humid conditions, it is necessary to prevent the substitution of oxygen species adsorbed on metal oxides by hydroxyl groups. This is an essential step to allow the gas sensors based on nano- and microstructures of metal oxides to be placed on the market.

Many studies were performed to eliminate the impact of water vapor on detector characteristics of metal oxide nano- and microstructures. For example, Kim et al. doped SnO_2 hierarchical structures with NiO and observed that a hydroxyl groups are absorbed by the NiO instead of SnO_2.[9] In this case, the NiO acts as hydroxyl groups absorber and the high gas response even in a humid atmosphere without sacrificing the response can be achieved.[9] The strategy to reduce the influence of water vapor on the gas response by adding water absorbers (CeO_2, CuO, Sb, Al, etc.) was used by Li et al.,[10] Choi et al.,[11] and Suematsu et al.[12,13] Another strategy was presented by Wang et al., which is based on creating a hydrophobic surface.[14] For example, the NiO structures covered with ZnO nanothorns were presented, which showed a low dependency of gas sensing properties for detecting NH_3 on the relative humidity.[14] Another example to cover the metal oxide nano- and microstructures with a thin SiO_2 absorber layer was presented by Gunji et al.[7] It was observed that nanofibers with core–shell SiO_2/SnO_2, grown by TEMPO-oxidized cellulose nanofibers as templates, demonstrated less influence of the H_2O poisoning compared to the uncovered SnO_2 nanoparticles.[7]

There have been many attempts to produce an optical gas sensor made of porous silicon. Although porous silicon gas sensors have a very large surface area, their long-term stability is affected by changes in the surface chemistry, for example, by temperature and humidity, leading to complete mechanical destruction of the gas sensor. Typical measures such as chemical functionalization or hydrogen termination did not lead to sufficient long-term stability of the porous silicon sensor. To replace the hydrogen-terminated surface, buffer layers of SiO_2 are developed, as shown in this study. Combining the large surface area of the here prepared ZnO sensors with a thin SiO_2 top-layer makes it possible to overcome the long-term stability problem.

Another important challenge for the mass production of gas sensors based on metal oxides is the unavoidable changes in the chemical and structural performances of materials due to operation at high temperatures.[5,7,9,15,16] While the mean time between failure of the standard electronics nowadays is longer than 200 years, the gas sensors will not last as long.[17] The lifespan of a sensor depends on several factors: i) used technology; ii) environmental conditions (humidity, temperature, etc.); and iii) gas exposure (the type of gas—reducing or oxidizing, the concentration of gas, etc.).[17] For example, electrochemical sensors for CO and H_2S gases have a lifetime typically of 2–3 years, while HF gas sensors have a lifetime of 1–1.5 years only.[18] In most cases, the stability of metal oxide nano-microstructures is measured during a period of 30–60 days.[16,19] To the best of our knowledge, there are only a few studies on the time-dependent stability of gas sensing devices. For example, Ozaki et al. investigated the long-term stability of SnO_2 structures modified by H_2SO_4 over 550 days.[20] The treatments with H_2SO_4 were applied in two ways: i) kneading of SnO_2 powders with a H_2SO_4 solution; or ii) dipping of the gas sensor in the solution.[20] Both methods enhanced the response to carbon monoxide and hydrogen.[20] In another study, Romain and Nicolas evaluated the performance of Figaro type gas sensors during a period of >3 years, where two identical sensor arrays worked continuously without interruption.[21] Furthermore, they observed the drift of sensors for a period of 7 years,[21] as well as the discrepancy in the temporal comportment of identical sensors and the effect of sensor replacement on the e-nose results.[21] Therefore, such studies have an important role in the determination of future perspectives for gas sensors made of nano- and microstructures of metal oxides. Especially when using these sensors in combination with Li-ion batteries, their long-term stability is most important since batteries with a liquid electrolyte using lithium are still very reactive.

In this work, the increase of time-dependent stability of sensing devices based on undoped and doped ZnO structures was achieved by coating the samples with an ultra-thin SiO_2 layer using an atmospheric pressure plasma jet.[22] The role of the SiO_2 ultra-thin layer is to adsorb the water-driven species and to avoid the hydroxyl poisoning of the ZnO samples. The UV and gas sensing measurements were performed for a relatively long period of time, namely for ≈7 months (203 days). Conduction of both types of measurements, that is, gas and UV sensing, is dictated by the necessity of multifunctional devices with simple fabrication methods and the ability to monitor multiple ambient parameters simultaneously, which would make them highly attractive from the economic and timesaving point of view.[23] In this case, it is not necessary to place the UV photodetector into a vacuum. The studies were carried out under different ambient conditions in order to examine the impact of the top SiO_2-layer on the long-term stability of ZnO with various dopants such as Cu, Sn, and Ag. These measurements are essential for the determination of reliability and stability of sensors, especially for those based on nano- and microstructures of metal oxides since they require a relatively high working temperature for adequate detection of gaseous species.

2. Results and Discussions

2.1. Characterization of SiO_2-Covered ZnO Columnar Films

The fabrication procedure of the investigated devices is illustrated in Figure S1, Supporting Information, and can be described as follows: i) the cleaning and sensitization of a glass substrate using $SnCl_2$/HCl solution as was described previously;[2,24] ii) chemical solution synthesis (SCS) deposition of columnar zinc oxide films with a thickness of 1.35–1.6 µm (see Figure S2a,b, Supporting Information); iii) deposition of an ultra-thin SiO_2 layer of 10 or 20 nm thickness using the plasma jet; and iv) deposition of gold contacts sustained through a metallic shadow mask with the configuration of a meander having 1 mm in width forming the Au/SiO_2/ZnO/SiO_2/Au structure with ohmic contacts.[3] The surface morphology of SiO_2-covered ZnO columnar films was investigated using scanning electron microscopy (SEM). **Figure 1** and Figure S2c, Supporting Information, show the SEM images of SiO_2-covered undoped, Sn-, Fe-, and Cu-doped ZnO columnar

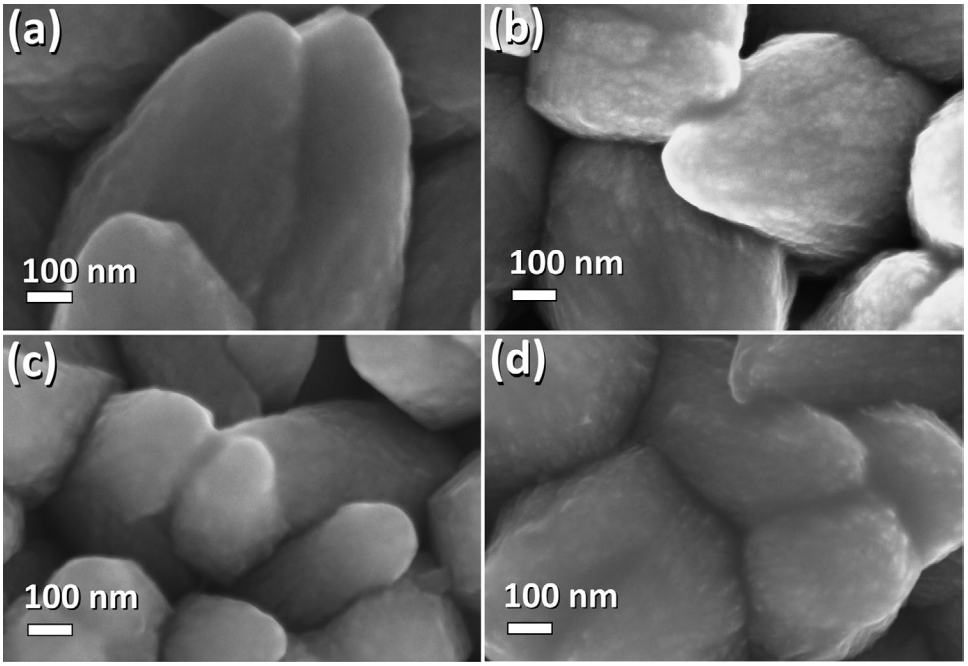

Figure 1. SEM images of SiO_2-coated ZnO columnar films: a) undoped, b) Sn-doped, c) Fe-doped, and d) Cu-doped.

films. Compared to SEM images of uncovered ZnO columnar films reported previously,[3,25–27] it can be observed that the ZnO grains are covered with a spider web-like layer. The presence of a covering layer is more evident at grain boundaries, especially at higher magnification (see Figure S2c, Supporting Information). In order to prove that the ultra-thin layer deposited using an atmospheric pressure plasma jet is SiO_2, that is, the oxidation state of Si is 4^+, the X-ray photoelectron spectroscopy (XPS) measurements of the coated ZnO columnar films sensor structures were carried out. XPS is a highly surface-sensitive technique, which can measure the elemental composition of the materials and is suitable for our purposes. The overview XPS spectrum of the ZnO with the SiO_2 layer on top is shown in **Figure 2**a. The peaks in the spectra correspond to the elements Na, Zn, O, Au, C, and Si. The Na originates most likely from the glass substrate, which contains Na. Due to the heat treatment, it is possible that the Na diffuses to the surface.[28] The C peak originates from adsorbed atmospheric hydrocarbons.[28,29] For a detailed XPS analysis, the C-1s, Si-2p, and Zn-2p were measured with a high resolution. The resulting spectra are shown in Figure 2b.

The C-1s spectrum was used for the calibration of all samples and is set to 285.0 eV (Figure 2b).[30] The Si-2p peak for pure Si is reported many times around 99 eV and the Si-2p peak for SiO_2 between 103.0 and 104.1 eV.[30,31] The high-resolution spectrum of the Si-2p shows that the peak is located at 102.9 eV, which indicates that Si is present in the oxidation state Si^{4+} and proves that SiO_2 was successfully deposited on top of the sample.

The high-resolution spectrum of the Zn-2p peaks shows that the Zn-$2p_{3/2}$ line can be found at 1022.7 eV, which indicates that the Zn is in the oxidation state Zn^{2+} in ZnO (Figure 2b). In metallic Zn, the Zn-$2p_{3/2}$ peak is expected to be located between 1020.8 and 1022.1 eV. In contrast, the Zn-$2p_{3/2}$ peak for ZnO

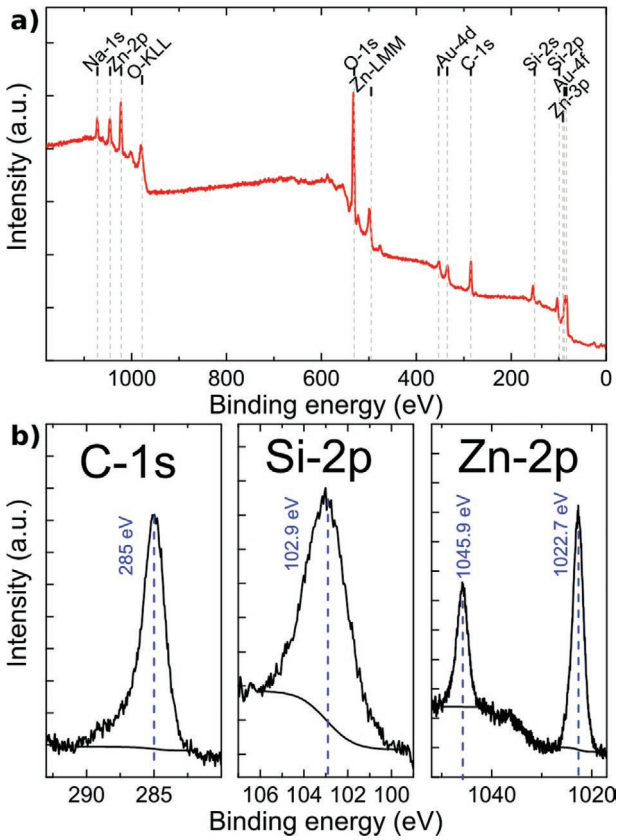

Figure 2. XPS spectra of ZnO with a SiO_2 coating. a) The overview spectrum shows the presence of Na, Zn, O, Au, C, and Si. b) The high-resolution spectra of the C-1s line, Si-2p line, and Zn-2p lines are shown. The peak locations of Si-2p and Zn-2p lines correspond to Si^{4+} in SiO_2 and Zn^{2+} in ZnO, respectively.

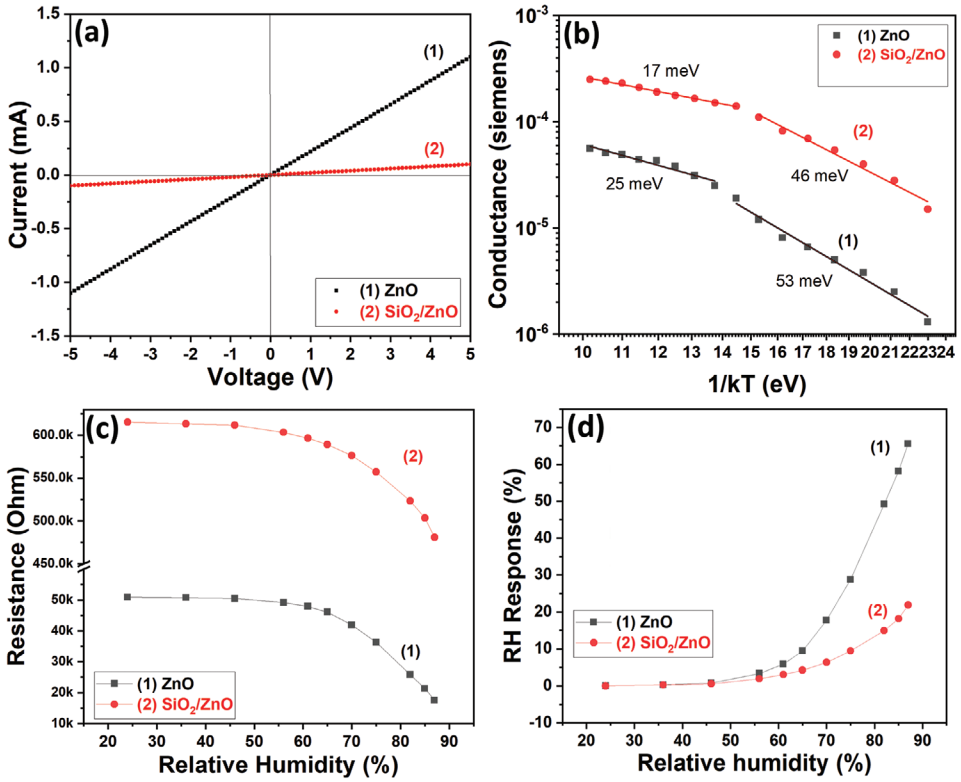

Figure 3. a) Current–voltage characteristics of the uncovered and SiO_2-covered ZnO columnar films. b) Arrhenius plot for the columnar ZnO and SiO_2-covered ZnO columnar films. Dependence of c) electrical resistance and d) RH response versus relative humidity for ZnO and SiO_2-covered ZnO columnar films with 10 nm thickness of SiO_2 top layer.

should be situated in the region from 1021.4 to 1022.5 eV, as reported in the literature.[30,31] Figure S3, Supporting Information, reports the X-ray diffraction (XRD) data of the SiO_2-covered ZnO, ZnO:Sn, ZnO:Cu, and ZnO:Ag columnar films, studied at room temperature after the deposition of the gold contacts. Therefore, the detected peaks can be attributed to the hexagonal wurtzite structure of ZnO, as well as to the cubic Au with the space group *Fm-3m* (no. 225). No diffractions corresponding to SiO_2 were detected, which is either due to the low XRD instrumental detection limit or an indication of an amorphous state of the deposited ultra-thin layer.

After identification of successful deposition of the SiO_2 layer on the top of ZnO columnar films, the fabricated sensor structures were characterized by electrical measurements to investigate the impact of the SiO_2 layer on the resistance of the overall structure. **Figure 3**a presents the current–voltage characteristics of uncovered and SiO_2-covered ZnO columnar films. It can be observed that SiO_2-covered films show lower current values (about one order of magnitude), which can be attributed to the insulating properties of the SiO_2 top layer.[7] Figure 3b shows the Arrhenius plot of electrical conductance (vs $1/kT$, where k is the Boltzmann constant and T is the absolute temperature) for the uncovered ZnO and SiO_2-covered ZnO samples. For investigated specimens, double-valued activation energy was observed. Therefore, the electrical conductivity is described by[32]

$$\sigma = \sigma_1 \exp\left(-E_{a1}/kT\right) + \sigma_2 \exp\left(-E_{a2}/kT\right) \quad (2)$$

where E_{a1} and E_{a2} is the activation energy for the conduction band and for the nearest neighbor hopping conduction, while σ_1 and σ_2 are the pre-exponential factors.[32] The results for E_{a1} of 25 and 17 meV were found for zinc oxide and for SiO_2-covered ZnO, respectively, which is similar to results obtained for other ZnO structures.[32,33] The E_{a2} value of 53 and 46 meV were determined for zinc oxide and for SiO_2-covered ZnO, respectively, and were attributed to the thermionic emission over grain boundaries.[32,33]

2.2. Dependence on Relative Humidity

The dependence of the electrical resistance on the relative humidity (RH) is shown in Figure 3c. From these measurements, the RH response of ZnO and SiO_2/ZnO samples was calculated and presented in Figure 3d. As can be observed, the lowest resistance dependency on RH was demonstrated by SiO_2-coated samples. Moreover, with an increase of the top SiO_2 layer thickness from 10 to 20 nm, a further increase in immunity to RH was obtained. Therefore, the ZnO columnar films demonstrated a RH response of ≈65.5% to ≈87% RH, while SiO_2-coated ZnO columnar films demonstrated a response of ≈21% and ≈18% for the layer thickness of 10 and 20 nm, respectively. The significant impact of RH on electrical resistivity is widely studied, and many humidity sensing devices have been developed on ZnO structures.[34] In our case,

by coating the surface with an ultra-thin layer of SiO_2, the partial decreases in adsorption sites for hydroxyl groups can be obtained, which efficiently decreases the resistance dependence on water vapor. However, the thicker SiO_2 top layer can lead to a considerable reduction in adsorption sites on the upper layers of ZnO and, therefore, to a significant reduction of gas sensing properties.

2.3. The Long-Term Stability of SiO_2-Coated ZnO Columnar Films

Next, the electrical, UV, and gas sensing experiments were performed for a relatively long period of time, namely for ≈7 months (203 days) at different ambient conditions, to investigate the impact of top SiO_2-layer on long-term stability for different ZnO samples doped with Cu, Sn, and Ag. The long-term current–voltage (I–V) curves of SiO_2-coated ZnO and doped ZnO (Sn, Cu, and Ag) columnar films are presented in Figure S4, Supporting Information. It can be observed that during the 203 days for all samples, except for SiO_2/ZnO:Cu, the electrical current is increasing with time. This can be attributed to the deposition of adventitious carbon, hydrocarbons, and carbonyl compounds, that is, surface contaminations from the atmosphere.[3,25] X-ray spectroscopy measurements in previous studies demonstrated that keeping the samples in ambient air during 1 month results in a deposition of ≈30% of adventitious carbon.[3,25] This can decrease the electrical resistance of samples with time. To verify this, the electrical resistivity of samples from current–voltage characteristics at an applied bias voltage of 5 V was determined. The conductance of the grain network (G) can also be calculated using the following equation[19]

$$G \propto \frac{q\mu_0 N_d (D-W)^2}{l} \exp\left(-\frac{qV_s}{kT}\right) \quad (3)$$

where μ_0 is the electron mobility of crystal, l is the interelectrode distance, D is the diameter of grains, q is the electron charge, W is the width of space charge region, V_s is the surface potential, and N_d is the donor concentration. However, because a series of parameters cannot be calculated and measured precisely, it was assumed that samples are composed of a continuous film, and the electrical resistivity was calculated using a standard formula for a conductor.

The results of the electrical resistivity measurement are presented in **Figure 4**a. The relative change in electrical resistivity was calculated using the following equation

$$\frac{\Delta\rho}{\rho} = \left|\frac{\rho_0 - \rho}{\rho_0}\right| \times 100\% \quad (4)$$

where ρ_0 is the electrical resistivity measured on the day of the sample preparation. The data for uncoated, SiO_2-coated ZnO and doped ZnO columnar films were plotted in the same graph in Figure 4a in order to be easily compared to each other. It is clearly observable that SiO_2-coated samples show higher stability in time compared to uncoated samples.

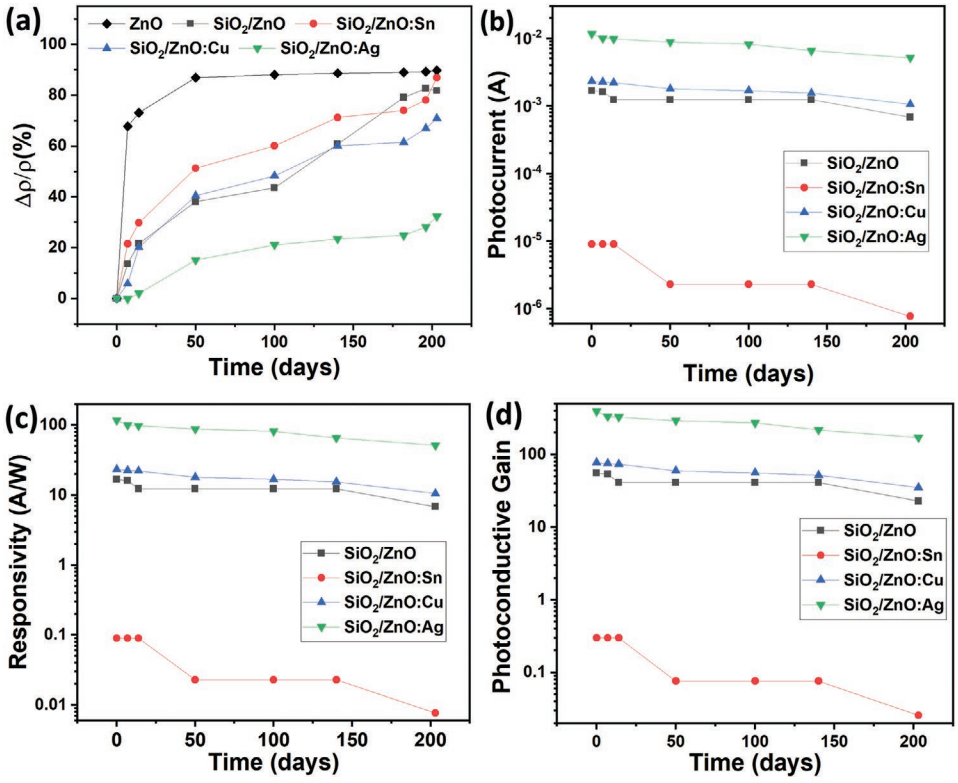

Figure 4. The change in: a) electrical resistivity, b) photocurrent value (under UV illumination), c) responsivity, and d) photoconductive gain of columnar films (SiO_2/ZnO, SiO_2/ZnO:Sn, SiO_2/ZnO:Cu, and SiO_2/ZnO:Ag) over time at room temperature.

In order to draw conclusions from these data, the influence of doping on the electrical resistance of columnar films need to be discussed. Fan and Freer observed that grain and grain boundary resistance increases with the rise in Ag concentration and suggested that Ag^{1+} could substitute Zn^{2+} in ZnO, which can be represented as follows[35]

$$2Ag \xrightarrow{ZnO} 2Ag'_{Zn} + V_O^{\cdot\cdot} \quad (5)$$

where $V_O^{\cdot\cdot}$ is a double ionized oxygen vacancy.

Because the Ag acceptors are formed in the ZnO matrix, the electrical resistance of ZnO:Ag columnar film grains is increased. Ag^{1+} may also behave like an amphoteric dopant, suggested as[36]

$$2Ag \xrightarrow{ZnO} Ag'_{Zn} + Ag_i^{\cdot} \quad (6)$$

In the case of doping with Cu, the increase in resistivity may be explained by the following equation[37]

$$CuO \xrightarrow{ZnO} Cu'_{Zn} + O_o^x + h^+ \quad (7)$$

Therefore, the holes are generated, which recombine with free electrons from ZnO and increase the electrical resistivity. Generally, the Cu-doping of ZnO (ZnO:Cu) is an excellent method to tune the conductivity.[29] A model for the formation of donor–acceptor pair for Cu_{Zn} was already described by[29,38]

$$Cu_{Zn}^* + Zn_i^* \rightarrow [Cu_{Zn} - Zn_i]^x \quad (8)$$

Therefore, the incorporation of Cu into the ZnO matrix introduces deep acceptor levels, which is confirmed by photoluminescence studies.[29]

On the other hand, in the case of doping with Sn, the decrease in electrical resistance originates from the generation of a higher amount of free electrons as a result of the higher valence of Sn^{4+}, which substitute Zn^{2+} ions in ZnO and form a double-donor state with injection of two electrons ($Sn_{Zn}^{\cdot\cdot} + 2e^-$).[39,40]

It is known that the Debye length (d) is reduced at a higher concentration of charge carriers (n_e) (see Equation (9)). The change of region with electron depletion under desorption/adsorption of oxygen will be lowered, producing smaller responses to UV light[25,41]

$$d = \left(2\varepsilon_0\varepsilon_s V_s / q n_e\right)^{1/2} \quad (9)$$

where ε_0 is the dielectric constant, ε_s is the permittivity of ZnO, and V_S is the induced band bending based on oxygen species adsorption.

Therefore, based on data from Figure 4a, we can tentatively propose that in the case of layers with lower electrical resistivity (in our case, the SiO_2-coated ZnO and Sn-doped ZnO columnar films), the deposition of adventitious carbon on the surface[3,25] leads to more significant changes compared to those with higher resistivity after doping with Ag and Cu. Thus, the use of films with higher resistivity can be more favorable for long-term applications such as gas sensors or UV photodetectors.

2.4. UV Sensing Measurements at Room Temperature

Figure S5, Supporting Information, presents the measured current–voltage characteristics at room temperature under UV light illumination for SiO_2/ZnO, SiO_2/ZnO:Sn, SiO_2/ZnO:Cu, and SiO_2/ZnO:Ag samples. The UV sensing characteristics of ZnO:Fe were studied in the previous work,[3] and were not included in the present UV sensing studies. These characteristics were also measured during 203 days, showing the decrease in current during time. However, these characteristics do not reflect the value of photocurrent due to the variation of dark current. Therefore, we calculated the value of photocurrent (I_{ph}) for all samples using the following equation

$$I_{ph} = I_{UV} - I_{dark} \quad (10)$$

where I_{UV} and I_{dark} represent the electric current of sensor structures under illumination with UV light and exposure in the dark, respectively. The results are shown in Figure 4b.

From Figure 4b, it can be observed that a decrease in photocurrent values is due to an increase of dark current. In the case of SiO_2/ZnO:Sn, a decrease in photocurrent of approximately one order of magnitude was observed. The change in photocurrent value during 203 days for SiO_2/ZnO, SiO_2/ZnO:Sn, SiO_2/ZnO:Cu, and SiO_2/ZnO:Ag is ≈59%, ≈91%, ≈54%, and ≈56%, respectively.

The calculated long-term responsivity of the samples (SiO_2/ZnO, SiO_2/ZnO:Sn, SiO_2/ZnO:Cu, and SiO_2/ZnO:Ag) is presented in Figure 4c. The relative change in responsivity for these samples is the same as in the case of the photocurrent. The same holds for the value of the photoconductive gain, which is shown in Figure 4d. It can be shown that SiO_2/ZnO:Cu and SiO_2/ZnO:Ag can achieve a photoconductive gain higher than 100, which is very promising for UV sensing applications. This can be attributed to the high value of photocurrent.

Next, the dynamic response to UV light of SiO_2/ZnO, SiO_2/ZnO:Sn, SiO_2/ZnO:Cu, and SiO_2/ZnO:Ag columnar films was investigated to evaluate its maximal value and to determine the time constants of rising and decaying photocurrents. The UV dynamic response was measured at 30% and 75% RH using the protocol from Figure S6, Supporting Information. According to this figure, the first pulse of UV light is applied at an exposure of photodetector in ambient air with 30% RH. After this pulse, the RH is increased using a bubbler to 75%. After that, the second pulse of UV light is applied. In this way, the impact of RH on UV detection characteristics of SiO_2-coated columnar zinc oxide films can be evaluated. The duration of a UV light pulse is 120 s, while the time between pulses was set to 500 s due to a slow recovery of the samples. As will be presented, all samples have an incomplete recovery of the photocurrent, that is, they show persistent photoconductivity. Therefore, the photocurrent did not recover even after hours. Due to the incomplete recovery of the decaying photocurrent, it is hard to determine the correct time components (τ_{d1} and τ_{d2}). Therefore, only the information on the constant for rise time (τ_{r1} and τ_{r2}) photocurrent will be presented.

Figure 5 presents the UV dynamic response of SiO_2/ZnO, SiO_2/ZnO:Cu, and SiO_2/ZnO:Ag columnar films, measured according to the protocol from Figure S6, Supporting Information. The SiO_2/ZnO:Sn samples were not investigated due to

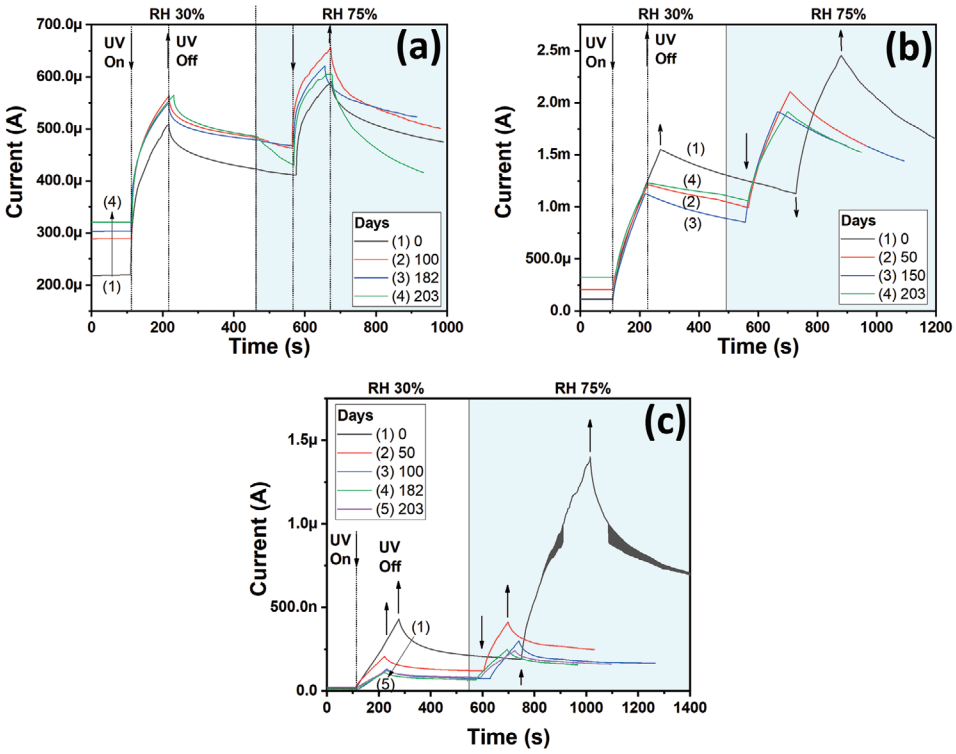

Figure 5. The dynamic UV response of: a) SiO_2/ZnO, b) SiO_2/ZnO:Cu, and c) SiO_2/ZnO:Ag columnar films at 30% and 75% relative humidity.

the low UV sensing properties. As can be observed, all samples show high values of persistent photoconductive currents after switching off the UV light source. Even after several hours, the decaying photocurrent does not recover to the starting electrical baseline. For SiO_2/ZnO columnar films, it can be observed that after the introduction of a higher concentration of water vapor in the test chamber (up to 75% RH), no essential changes in the electric current values occur for measurements up to 182 days. However, after 203 days, the changes can be observed (see Figure 5a). These results demonstrate the high immunity of SiO_2-coated samples to water vapor. For SiO_2-coated doped samples (SiO_2/ZnO:Cu and SiO_2/ZnO:Ag columnar films) even after 203 days, no observable changes in electric current after the introduction of a higher content of water vapor were noted. These results demonstrate that doping of samples with Ag^{1+} and Cu^{1+} can further improve the immunity of SiO_2-coated samples to water vapor.

Due to the incomplete recovery of the photocurrent, the second pulse generates values higher than that for the first pulse. However, even at high values of RH the samples respond to UV light. The calculated values of UV response at 30% and 75% RH are presented in **Figure 6**. The UV response for the first pulse was determined by

$$S_{UV} = \frac{I_{UV}}{I_{dark}} \tag{11}$$

The UV response for the second pulse was calculated using the same equation, but for I_{dark} the value of photocurrent before switching to the second pulse was chosen.

From Figure 6a, it can be seen that the responses to UV are decreasing with time, as well as all parameters investigated before (i.e., responsivity, photocurrent, and internal photoconductive gain). The highest UV response was found for SiO_2-coated ZnO:Ag columnar films. In this case, the UV response decreased from ≈22.4 to ≈5.2 after 203 days. The UV response for SiO_2-coated ZnO:Cu columnar films decreased from ≈14.6 to ≈3.8, while for SiO_2-coated ZnO columnar films, a decrease from ≈2.3 to ≈1.77 was observed. It is evident that doping with Ag and Cu not only improves the long-term stability but also efficiently increases the UV response.

In the case of the second pulse applied after a rise in the concentration of water vapor (75% RH), the UV response is respectively lower (as already mentioned before, it is due to the persistent photoconductivity). For SiO_2-coated ZnO:Ag columnar films, the UV response decreased from ≈7.5 to ≈3 after 203 days of keeping it in ambient air. For SiO_2-coated ZnO:Cu and ZnO columnar films, the UV response decreased from ≈2.3 to ≈1.8 and from ≈1.44 to ≈1.32, respectively (see Figure 6b). In order to evaluate the response time of elaborated photodetectors, the time constants of rising photocurrent were determined and presented in Figure S7, Supporting Information.

2.5. UV Sensing Mechanism in Humidity Conditions

The UV detecting mechanism of ZnO structures in dry and wet air was proposed in recent investigations.[25] However, from the experimental results, it was observed that the presence of SiO_2

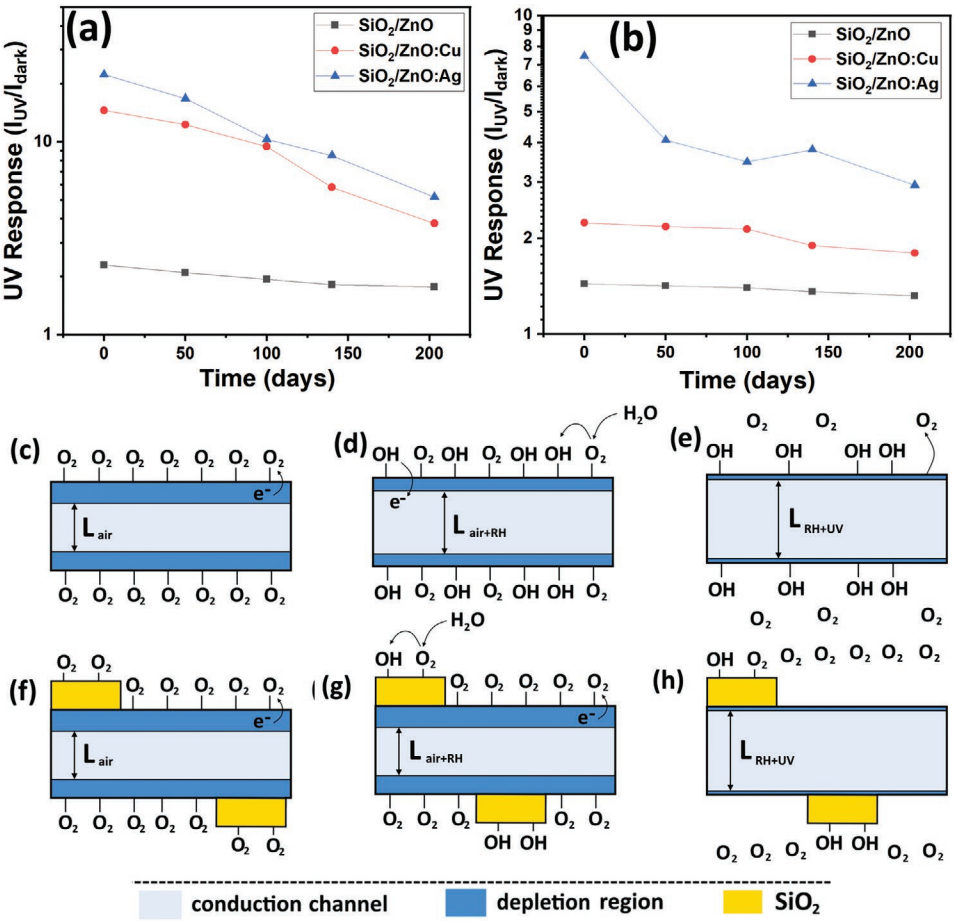

Figure 6. The calculated UV response for SiO_2/ZnO, SiO_2/ZnO:Cu, and SiO_2/ZnO:Ag columnar films at: a) 30% and b) 75% relative humidity. c–e) Illustration of influence on ZnO of the water vapor at room temperature and f–h) SiO_2/ZnO. Exposure under air without water vapor (c,f); exposure under air with a high concentration of water vapor (d,g); illumination with UV light (e,h).

ultra-thin layer induces a high immunity of ZnO columnar films to high concentrations of water vapor. Figure 6c–h shows a schematic model of the hydroxyl and oxygen co-adsorption on the top of ZnO and SiO_2/ZnO structures. In the presence of humidity, the hydroxyl groups are adsorbed on the ZnO surface that results in changes in the conduction channel L_{air} width (see Figure 6c,d). With an increase of water vapor concentration, the adsorption of O species is highly decreased due to the hydroxyl poisoning and leads to a narrowing of the conduction channel width ($L_{air + RH}$, see Figure 6c,d). Thus, less photogenerated holes will diffuse to the surface in order to discharge O_2^- by surface electron–hole recombination, which in its turn results in a reduction in the modulation of the conduction channel and leads to a loss in the UV response (see Figure 6e).[42–44]

In the case of SiO_2/ZnO structures (see Figure 6f,g), the hydroxyl groups are adsorbed mainly on the upper layers of the SiO_2, maintaining the adsorption of O_2^- even at high concentration of water vapor (in our case, even at 80%). Many studies demonstrated that SiO_2 is the ideal candidate for applications where water adsorption is necessary, including dehumidification systems.[45] For example, Hormádko et al. synthesized highly porous SiO_2 fibers by centrifugal spinning with high performances for adsorption of H_2O.[45] The theoretical studies (mainly DFT calculations) of H_2O adsorption on the silicon dioxide surface showed that H_2O is dissociated and causes the hydroxylation at the interface.[46,47] The high concentration of hydroxyl groups leads to an interface with hydrophilic properties.[48] Thus, we believe that the SiO_2 ultra-thin layer acts as a hydroxyl absorber by preferential capture.[9,12] As a result, the high modulation of the conduction channel under UV illumination is maintained (see Figure 6h).

2.6. Gas Sensing Measurements

The elaborated SiO_2-coated ZnO and doped ZnO columnar films were measured as gas sensor devices during the same period of time (203 days) in order to evaluate their long-term stability. All samples were kept in ambient air during this time in order to simulate the operation in real conditions. For these experiments, another set of samples was used (not the one used for UV sensing measurements). Based on the already reported gas sensing characteristics of the studied samples

(ZnO, ZnO:Sn, and ZnO:Fe columnar films),[3,25] several conclusions can be made:

i) The ZnO, ZnO:Sn, and ZnO:Fe columnar films are highly selective to VOCs vapors in a temperature range from 250 to 350 °C;
ii) The increase of water vapor concentration in the test chamber leads to a high loss in response due to hydroxyl poisoning.

In the measured operating temperature region, the SiO_2/ZnO:Cu samples demonstrated poor gas sensing properties to the tested gases/vapors (<1.2), while for SiO_2/ZnO:Ag samples, another method based on surface decoration was elaborated to improve gas sensing properties and immunity to water vapor.[26,49] Therefore, these samples were excluded from gas sensing measurements.

The long-term gas sensing performance of SiO_2/ZnO:Sn and SiO_2/ZnO:Fe columnar films was studied for 203 days at a working temperature of 300 °C. Several types of VOCs vapors, namely acetone, ethanol, and *n*-butanol vapors, were investigated. All samples were kept in the dark conditions in ambient air during the whole period of 203 days and were thermally exposed only during the measurements.

First of all, the long-term stability under ambient air conditions is evaluated. The long-term stability of gas sensing devices is of high importance, especially in battery technology and application.[49] A typical lifetime of batteries is around 5000–10 000 charging and discharging cycles, during which usually some non-predictable reactions/parasitic effects evolve or develop.

Consequently, it is highly necessary to have a long-term stable and very sensitive sensor to react and warn before the battery starts to degrade and stop working. **Figure 7**a shows the evolution in time (during 203 days) of gas response for ZnO:Sn, ZnO:Fe, SiO_2/ZnO:Sn, and SiO_2/ZnO:Fe columnar films to 50 ppm of ethanol vapor. During all measurements, the RH varied in the 30–40% range. As can be observed, the uncoated ZnO:Sn and ZnO:Fe columnar films have higher gas response compared to SiO_2-coated samples. For example, on the day when the samples were prepared, the gas response of ZnO:Sn, ZnO:Fe, SiO_2/ZnO:Sn, and SiO_2/ZnO:Fe columnar films to 50 ppm of ethanol vapor is 17, 16, 8, and 4.1, respectively. Therefore, the response for Sn-doped samples coated with SiO_2 was reduced by about 2 times, while for Fe-doped samples, the gas response was reduced by about 4 times.

However, it can be seen that the gas sensitivity of uncoated samples is highly reduced after 203 days, while for SiO_2-coated samples (≈10 nm), the gas response is only slightly reduced. For example, for ZnO, ZnO:Sn, and ZnO:Fe the gas response is reduced from 7.9, 17, and 16 to 2.6, 4.4, and 1.66 (by about 3, 4, and 10 times), respectively, after 203 days. For SiO_2-coated ZnO, ZnO:Sn, and ZnO:Fe samples, the gas response is slightly reduced from 3.2 to 2.1, from 8 to 4, and from 4.1 to 2.55, respectively, that is, by about 1.5, 2, and 1.6 times. After calculating the loss in response after 203 days (P_{time}) using Equation (12), it becomes apparent that SiO_2-coated samples show more stability, as can be seen from Figure 7b.

$$P_{time} = 100\% - \left((100\% \times S_0)/S\right) \quad (12)$$

where S_0 is the response measured on the day when the samples were prepared. As can be observed from Figure 7b, the loss in response for undoped samples is lower compared to ZnO:Fe and ZnO:Sn. This can be tentatively explained based on a higher concentration of oxygen vacancy defects for doped samples, observed in previous works by investigations of optical properties.[3,25] Higher concentration of oxygen vacancy defects can lead to a higher gas response,[50,51] as well as to increase of OH surface species through the enhanced dissociation of water at the V_O sites,[52–54] that is, can lead to decrease in immunity to water vapor and the long-term stability.[3,25,50–54] The dynamic gas response to ethanol vapor for ZnO:Sn, SiO_2/ZnO:Sn, ZnO:Fe, and SiO_2/ZnO:Fe columnar films was measured at different time intervals, and the results are presented in Figure S8, Supporting Information.

It is worth mentioning that the same tendency, which can be seen in Figure 7a,b, was also observed for other VOCs vapors, such as acetone and *n*-butanol. Next, the impact of a higher concentration of water vapor on the gas detection response of the studied samples will be investigated. Figure S9a, Supporting Information, presents the calculated response to 200 ppm of acetone vapor at 300 °C versus RH (30%, 60%, and 80%), measured on the day when the samples were prepared. As can be shown, in the case of coated samples, the dependence of gas response on RH is lower compared to uncoated samples. The dynamic gas response for uncoated and SiO_2-coated ZnO:Sn is presented in Figure S9b,c, Supporting Information. The results from Figure S9b,c, Supporting Information, once again demonstrate the high immunity of SiO_2-coated samples to water vapor. In the case of samples with a thicker SiO_2 layer (≈20 nm), the decrease in gas response was reduced considerably and presents no interest for practical applications (see Figure S9d, Supporting Information). Therefore, the optimal thickness of SiO_2 layer was found to be ≈10 nm.

2.7. Gas Sensing Mechanism

A higher immunity of gas response to RH of SiO_2-coated ZnO columnar films can be interpreted based on the observed lower dependence of electrical resistance on RH, see Figure 3. The impact of H_2O vapor on the mechanism for gas detection of ZnO and SiO_2/ZnO is tentatively proposed in Figure 7c–f. Exposing the samples to dry air, the width of the conduction channel will be reduced due to O_2 adsorption ($O_{2(g)} + e^- \rightarrow O_{2(ad)}^-$).[42,55,56] When ZnO is placed in normal ambient air with a higher concentration of H_2O vapor, these H_2O species are adsorbed on its top surface in the molecular or OH form with the release of charge carriers and can displace the previously adsorbed O species and free electrons (see Figure 7c,d). It provides electrical conductivity changes, as well as widens the conduction channel ($L_{air + RH}$) in columns.[9,57] However, for SiO_2/ZnO, the SiO_2 ultra-thin acts as a hydroxyl adsorber, which ensures a site of oxygen adsorption and reaction on the surface in a humid environment (see Figure 7c,d) that produces modifications in the conduction channel.[12] The same phenomena were detected for tetrapods of Fe_2O_3/ZnO,[58] Al-doped SnO_2 NPs,[12]

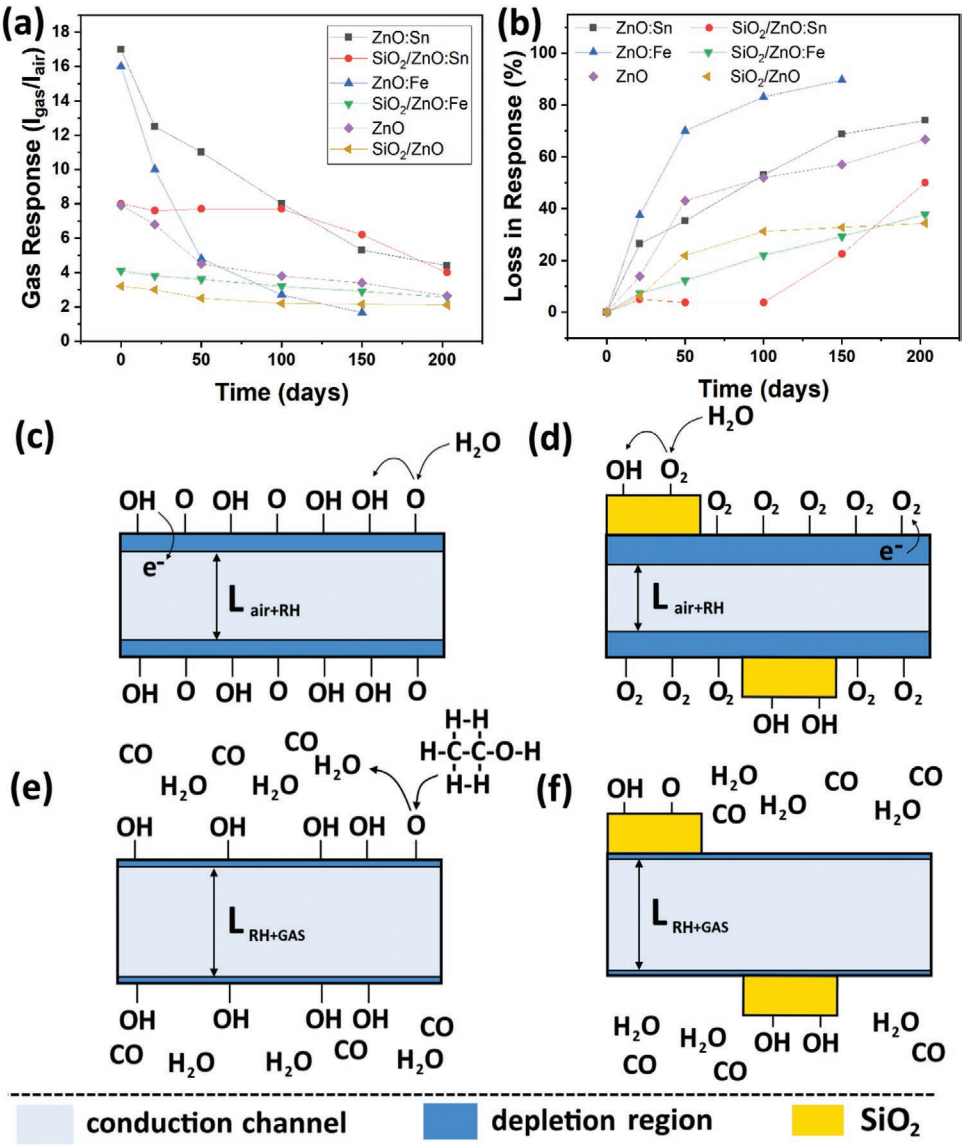

Figure 7. a) Gas response and b) loss in response versus time to 50 ppm of ethanol vapors for uncoated and SiO_2-coated (≈10 nm) ZnO, ZnO:Sn, and ZnO:Fe columnar films. Drawing of the H_2O vapor effect on ethanol vapor sensing of c,e) ZnO and d,f) SiO_2/ZnO. Exposure under air with a high concentration of H_2O vapor (c,d); introduction of ethanol vapor (e,f).

Sb-doped SnO_2,[13] CuO-loaded SnO_2 hollow spheres,[11] and NiO-doped SnO_2.[9]

Once ethanol vapor is introduced into the measurement chamber, the oxidation of ethanol takes place.[9,57] Next, the charge carriers are released into ZnO and widen the electrical conduction channel (L_{RH+gas}, see Figure 7e,f). Nevertheless, for specimens SiO_2/ZnO, the modulation of the channel for electrical conduction of these charges ($L_{air+RH} - L_{RH+gas}$) will be increased due to the lack of impact of H_2O vapor on conduction channel in ambient air with high RH value. Thus, the addition of the SiO_2 ultra-thin layer can reduce the effect/impact of H_2O vapor on gas detection characteristics of columnar ZnO films, which is highly necessary for real-life applications in a humid environment.

2.8. DFT Calculations: SiO_2:ZnO(0001) Surface and Molecule Interactions

DFT calculations as described in Computational Details (Text S1, Supporting Information) were performed. The bulk wurtzite structure of ZnO was optimized, as was reported previously.[59–61] The surface energy using a combination of computations for the relaxed and unrelaxed surfaces (details are given in previous works[59–61]) was calculated and the value of 2.28 J m^{-2} was obtained. Zn-terminated polar (0001) surfaces have been found to be very active surfaces and studied extensively for gas sensing and catalytic experiments.[60,62] In the case of SiO_2:ZnO(0001) surface model, we substituted two Zn atoms in the top surface layer with a Si atom to maintain the charge

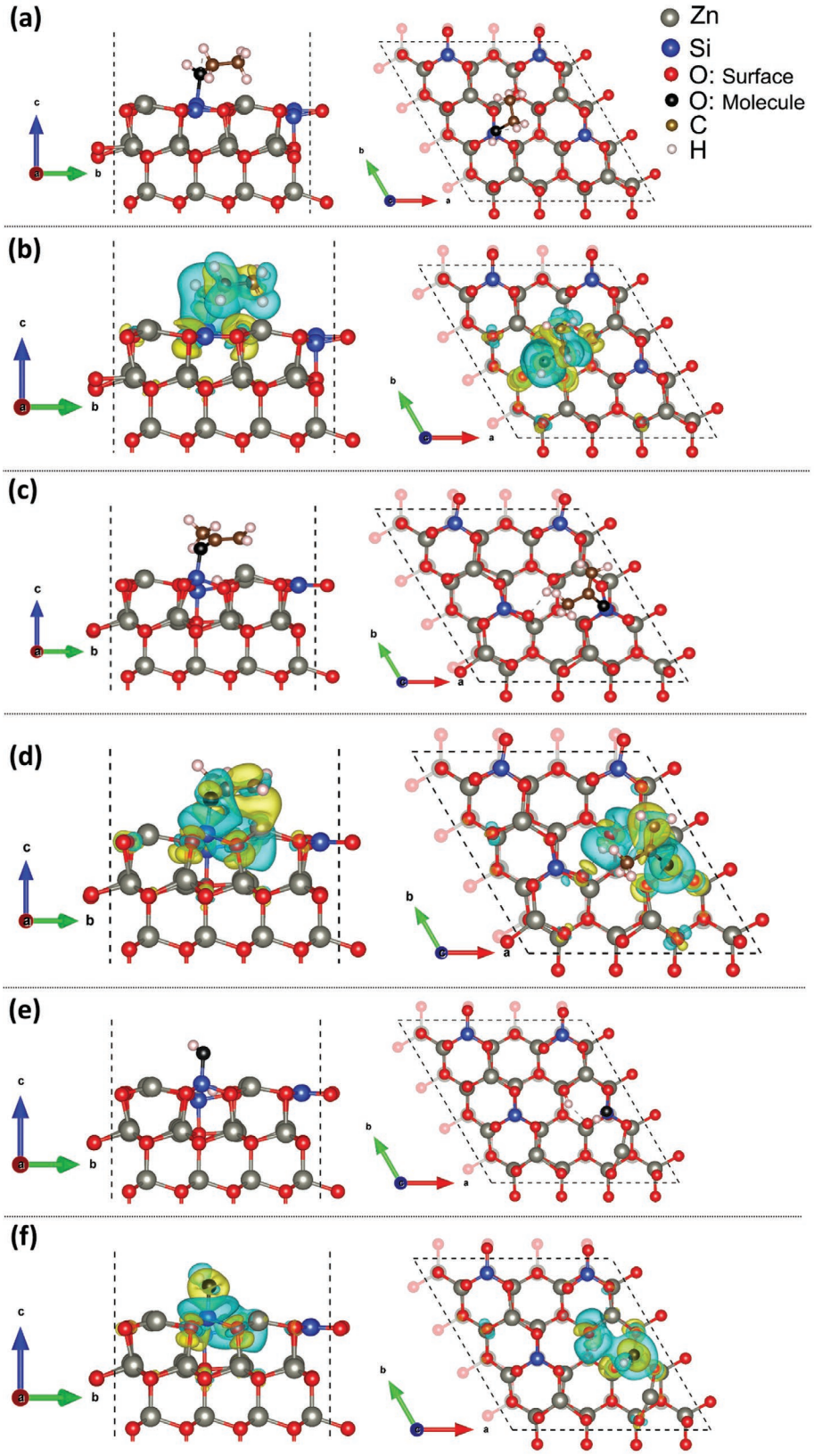

Figure 8. Interaction of a) ethanol, c) acetone, and e) water molecule with SiO_2:ZnO(0001) surface. Charge density difference plot of b) ethanol, d) acetone, and f) water molecule interaction on the SiO_2:ZnO(0001) surface, where positive and negative charge densities in (e $Bohr^{-3}$) are indicated by yellow and blue colors.

neutrality. We tried four possible configurations and found the most stable structure, as shown in Figure S11, Supporting Information, where Si atom connects with four O atoms in the top layer, with Si—O bond lengths of 1.62, 1.57, and 1.62 Å, whereas surface Zn atom forms Zn—O bonds of 2.07, 1.82, and 2.07 Å, as shown in Figure S10, Supporting Information.

In the next step, we investigated the interaction of an ethanol molecule with the SiO_2:ZnO(0001) surface. As shown in **Figure 8**a, the ethanol molecule interacts strongly with the surface where the oxygen atom of the molecule binds with the surface Si atom with a bond length of 1.83 Å. The calculated binding energy was found to be –1.95 eV. The Bader charge analysis (Figure 8b) shows that the 0.043 e^- charge is transferred from the molecule to the surface (Table S1, Supporting Information). Figure S11, Supporting Information, presents the partial density of states for SiO_2:ZnO(0001) surface with ethanol molecule, where a change in intensity of electronic bands is observed due to this strong interaction of ethanol molecule with the surface. Also, the Fermi energy of the surface is changed from –2.787 to –2.515 eV after ethanol molecule interaction.

We placed acetone molecule in different orientations close to surface sites available on the SiO_2:ZnO(0001) surface. As presented in Figure 8c, the acetone molecule is dissociated on the surface with the adsorption energy of –5.10 eV, where the O atom of the molecule binds with the surface Si atom with the bond length of 1.70 Å and hydrogen atom binds with surface O with the bond length of 0.99 Å. The calculated results of the Bader charge analysis (Figure 8d) show that the 0.051 e^- is transferred from the molecule to the surface (see Table S2, Supporting Information). Figure S12, Supporting Information, presents the partial density of states for SiO_2:ZnO(0001) surface with the acetone molecule, where the Fermi energy of the surface is changed from –2.787 to –2.648 eV after acetone interaction.

We also investigated the water adsorption on the SiO_2:ZnO(0001) surface, and our calculations show that as soon as the water molecule comes into contact with this surface, the molecule is dissociatively adsorbed on the SiO_2 layer as illustrated in Figure 8e. Water species binds very strongly to the SiO_2 layer with a binding energy of –4.15 eV, as OH species bind with the surface Si atom with a bond length of 1.65 Å, and the H atom binds with the surface O atom with a bond length of 0.99 Å. The Bader charge analysis is performed (Figure 8f), and the calculated results showed that –0.129 e^- charge is transferred from the surface to the water molecule (see Table S3, Supporting Information). Figure S13, Supporting Information, presents the partial density of states for SiO_2-ZnO(0001) surface with and without the water molecule, where Fermi energy of the surface alters from –2.787 to –2.871 eV after interaction with the water molecule.

The observed behavior of water dissociation is in contrast to the behavior on pristine ZnO (0001) surface, where water molecule interacts with the surface without dissociating molecularly with the binding energy of only –0.82 eV, as shown in Figure S14, Supporting Information.

3. Conclusion

The minimization of the hydroxyl poisoning effect is essential in order to achieve humidity-tolerant sensors that are able to work efficiently in ambient conditions. Since these sensors are very immune to humidity, they are optimal for applications, where it is: i) necessary to have a long-term stable measurement or sensitivity for specific gases; and ii) they can also be used as short-term sensors, for example, during the preparation of a battery anode in a dry room. In these conditions, it is essential to have dry air with very low humidity to avoid any unwanted reactions with the used anodes or cathodes. Using these sensors could lead to an early detection system in battery fabrication processes. The obtained results demonstrate the possibility to inhibit the hydroxyl poisoning of the undoped and doped ZnO columnar films (ZnO:Sn, ZnO:Fe, ZnO:Ag, and ZnO:Cu), synthesized by using a simple SCS approach by coating them with an ultra-thin layer of SiO_2. The XPS measurements demonstrated that Si is present in the oxidation state Si^{4+}, which proves that SiO_2 was successfully deposited on top of the sample using an atmospheric pressure plasma jet coating. The evaluated electrical, UV, and gas sensing properties under different ambient conditions for 203 days showed a higher immunity to water vapor and higher long-term stability for SiO_2-covered samples. The doping of samples with Ag^{1+} and Cu^{1+} can further improve the immunity of SiO_2-coated samples toward water vapor as well as to efficiently increase the UV response. It was observed that in the case of ZnO:Sn and ZnO:Fe structures, the gas response is reduced by about 75% and 90%, respectively, after 203 days, while for SiO_2 (10 nm)-coated ZnO:Sn and ZnO:Fe columnar films, the gas response is only slightly reduced by about 50% and 38%, respectively. The optimal thickness of SiO_2 layer was found to be ≈10 nm. Furthermore, it was observed that for coated samples, the dependence of gas response on relative humidity is lower compared to uncoated samples. DFT calculations suggest that the immunity of the SiO_2/ZnO system to H_2O is due to the strong adsorption of water vapor. In this case, the water vapors are preferentially adsorbed on SiO_2 and not ZnO. Thus, the ZnO grains, as well as gas sensing properties, remain unaffected by water vapor. Therefore, our findings regarding the surface coating of ZnO columnar films with an ultra-thin SiO_2 layer (10 nm) may allow a fabrication of humidity-tolerant UV photodetectors and gas sensor made of ZnO columnar films with excellent long-term stability.

4. Experimental Section

The undoped and doped ZnO columnar films (ZnO, ZnO:Sn, ZnO:Ag, and ZnO:Cu) were grown via the SCS approach, as previously reported.[3,25] The doping levels of 0.24 at% Fe, 0.4 at% Sn, 0.95 at% Ag, and 0.5 wt% Cu were achieved by adding 0.8 mM of [$Fe_2(SO_4)_3{\cdot}7H_2O$] (iron(III) sulfate hydrate), 11.5 mM of [$SnSO_4$] (tin (II) sulfate), 5.3 mM of [$AgNO_3$] (silver nitrate), and 8.5 mM of [$CuSO_4{\cdot}5H_2O$] (copper(II) sulfate pentahydrate) in complex solution, respectively, according to investigations from previous works.[3,25,26] The choice of these values was based on a higher sensing performance shown previously.[3,25,26] The detailed morphological, structural, and chemical properties of columnar ZnO films (undoped and doped) were published in the author's works,[3,25,26] which demonstrated that the films were composed of columnar grains with a diameter range of 200–400 nm and a thickness of ≈1.5 µm.

The SiO_2 ultra-thin layer (of 10–20 nm) was deposited on the top of samples using the commercial atmospheric pressure plasma jet PFW 10 (Plasmatreat GmbH, Steinhagen, Germany) and hexamethyldisiloxane

(HMDSO) as precursor similar as in other works.[63–66] The jet parameters were 300 V primary voltage, 19 kHz discharge frequency, and a plasma cycle time of 100%, which corresponds to a duty cycle of 50%. As working gas, 30 slm pressured air was used, and 1 slm N_2 (Air Liquide, 99.995% purity) was bubbled through the liquid HMDSO (Merck KGaA, GC, area% ≥ 98.5 area%). The precursor feed line was heated to 70 °C to avoid condensing. The prepared thin films were moved underneath the jet with a speed of 30 or 60 m min^{-1}, respectively, and a distance of 5 mm to the jet nozzle. The thin film thickness obtained by these parameters was determined by using a Si wafer as a substrate and a profilometer (Bruker DektakXT) for the measurements. The obtained SiO_2 film thicknesses on the Si wafers depend on the substrate speed of 30 or 60 m min^{-1} and were about 40 or 20 nm, respectively. Considering the non-uniform surface of the substrates and the fact that most samples were prepared at 60 m min^{-1}, the SiO_2 layer in this study was assumed to be deposited non-uniform with a thickness of about 10–20 nm, that is, SiO_2 layer was not continuous. The columns of the ZnO were coated individually, thus, the high porosity and 3D structures were preserved. For some spots, the columns were too close together, resulting in a merged SiO_2 layer while the ZnO below the coating stays separated.

The electrical measurements were measured and recorded on PC by the Keithley 2400 sourcemeter using a graphic user interface made in LabVIEW. The sensing properties to VOCs vapors were performed using the procedure described in previous works.[67,68] The information on computational details, namely DFT calculations, is presented in Text S1, Supporting Information, and similar to the previous works.[59–61]

For chemical composition identification of the ZnO coated with the SiO_2, one sample was investigated by XPS with an Omicron Nano-Technology GmbH XPS system (Al-anode, 240 W). The obtained data were analyzed with the software CasaXPS (version 2.3.18). The charging was corrected by calibrating the C-1s line of beneficial carbon contaminants to 285.0 eV.[30]

The relative humidity response (S_{RH}) was found as follows[69]

$$S_{RH} = \left(\frac{R_{RH0} - R_{RH}}{R_{RH0}}\right) \times 100\% \tag{13}$$

where R_{RH0} is the electrical resistance of a sensor structure at the minimum value of measured relative humidity (RH) of 20% and R_{RH} is the electrical resistance of a sensor structure at different values of RH. The self-build experimental setup used for the generation of different concentrations of water vapor using a water bubbling system is presented in Figure S15, Supporting Information. The sensor structures were placed in a sealed chamber, where the water vapor was transported. The RH value in the chamber was controlled continuously using a standard hygrometer. The ambient air with already 20–30% RH was used as a carrier gas.

Visible-blind UV photodetectors are an important application of ZnO films due to its large band-gap E_g = 3.37 eV at 300 K, and its fabrication represents an accessible technology. Therefore, the elaborated SiO_2-coated ZnO columnar films were investigated as UV photodetectors at room temperature. The UV light irradiance (λ = 365 nm) was established to ≈1 mW cm^{-2} using a UV light meter ST-513 from Sentry Optics. The UV detection studies were made at ≈25 °C (RT) in normal ambient air (relative humidity, RH ≈ 20%). The principal performances which depict the UV photodetectors performances are the R (responsivity) and G (the internal photoconductive gain), which were determined by[58]

$$R = \frac{I_{ph}}{P_{opt}} = \eta\left(\frac{q\lambda}{hc}\right)G \tag{14}$$

$$G \cong \frac{1}{L^2}\tau\mu_e V \tag{15}$$

where λ is the wavelength of UV light (365 nm), c is the speed of light, P_{opt} is the incident optical power, η is the quantum efficiency, h is Planck's constant, V is the applied bias voltage, L is the space between the electrodes, and μ_e is the mobility of electrons.[3,25]

Because the rising and decaying photocurrents have two components, that is, slow and rapid components, the time constants of rising (τ_{r1} and τ_{r2}) and decaying (τ_{d1} and τ_{d2}) photocurrents were determined using bi-exponential fit:[3,25,70]

$$I(t) = I_{dark} + A_1\left(1 - e^{-\frac{t}{\tau_{r1}}}\right) + A_2\left(1 - e^{-\frac{t}{\tau_{r2}}}\right) \tag{16}$$

$$I(t) = I_{dark} + A_3 e^{-\frac{t}{\tau_{d1}}} + A_4 e^{-\frac{t}{\tau_{d2}}} \tag{17}$$

where A_1, A_2, A_3, and A_4 are positive constants.

Supporting Information

Supporting Information is available from the Wiley Online Library or from the author.

Acknowledgements

O.L. acknowledges the Alexander von Humboldt Foundation for the research fellowship for experienced researchers 3-3MOL/1148833 STP at the Institute for Materials Science, Kiel University, Germany. Daria Smazna and Mathias Hoppe are acknowledged for support with SEM and contact deposition. L.H. and H.K. would like to thank Plasmatreat GmbH, Steinhagen, Germany for providing the plasma jet. Special thanks go to the Federal Ministry of Education and Research (BMBF) of Germany for partially funding this project within the project "PorSSi" (03XP0126 B). This work was partially supported by the Technical University of Moldova and through the ANCD-NARD Grant No. 20.80009.5007.09 at TUM.

Open access funding enabled and organized by Projekt DEAL.

Conflict of Interest

The authors declare no conflict of interest.

Data Availability Statement

Research data are not shared.

Keywords

gas sensors, long-term stability, nano-crystalline materials, UV photodetectors, ZnO columnar films

Received: November 13, 2020
Revised: January 26, 2021
Published online: March 18, 2021

[1] J. Zhang, X. Liu, G. Neri, N. Pinna, *Adv. Mater.* **2016**, *28*, 795.
[2] O. Lupan, L. Chow, S. Shishiyanu, E. Monaico, T. Shishiyanu, V. Şontea, B. R. Cuenya, A. Naitabdi, S. Park, A. Schulte, *Mater. Res. Bull.* **2009**, *44*, 63.
[3] V. Postica, I. Hölken, V. Schneider, V. Kaidas, O. Polonskyi, V. Cretu, I. Tiginyanu, F. Faupel, R. Adelung, O. Lupan, *Mater. Sci. Semicond. Process* **2016**, *49*, 20.
[4] M. Singh, N. Kaur, G. Drera, A. Casotto, L. Sangaletti, E. Comini, *Adv. Funct. Mater.* **2020**, *30*, 2003217.

[5] N. Bârsan, U. Weimar, *J. Phys.: Condens. Matter* **2003**, *15*, R813.
[6] M. Hübner, C. E. Simion, A. Tomescu-Stănoiu, S. Pokhrel, N. Bârsan, U. Weimar, *Sens. Actuators, B* **2011**, *153*, 347.
[7] S. Gunji, M. Jukei, Y. Shimotsuma, K. Miura, K. Suematsu, K. Watanabe, K. Shimanoe, *J. Mater. Chem. C* **2017**, *5*, 6369.
[8] W.-P. Tai, J.-H. Oh, *J. Mater. Sci.: Mater. Electron.* **2002**, *13*, 391.
[9] H.-R. Kim, A. Haensch, I.-D. Kim, N. Barsan, U. Weimar, J.-H. Lee, *Adv. Funct. Mater.* **2011**, *21*, 4456.
[10] H.-Y. Li, C.-S. Lee, D. H. Kim, J.-H. Lee, *ACS Appl. Mater. Interfaces* **2018**, *10*, 27858.
[11] K.-I. Choi, H.-J. Kim, Y. C. Kang, J.-H. Lee, *Sens. Actuators, B* **2014**, *194*, 371.
[12] K. Suematsu, N. Ma, M. Yuasa, T. Kida, K. Shimanoe, *RSC Adv.* **2015**, *5*, 86347.
[13] K. Suematsu, M. Sasaki, N. Ma, M. Yuasa, K. Shimanoe, *ACS Sens.* **2016**, *1*, 913.
[14] J. Wang, P. Yang, X. Wei, *ACS Appl. Mater. Interfaces* **2015**, *7*, 3816.
[15] A. Vergara, S. Vembu, T. Ayhan, M. A. Ryan, M. L. Homer, R. Huerta, *Sens. Actuators, B* **2012**, *320*, 166.
[16] N. Yamazoe, *Sens. Actuators, B* **2005**, *108*, 2.
[17] H. Wang, M. Liserre, F. Blaabjerg, *IEEE Ind. Electron. Mag.* **2013**, *7*, 17.
[18] E. Bakker, E. Pretsch, *Anal. Chim. Acta* **1995**, *309*, 7.
[19] V. V. Sysoev, T. Schneider, J. Goschnick, I. Kiselev, W. Habicht, H. Hahn, E. Strelcov, A. Kolmakov, *Sens. Actuators, B* **2009**, *139*, 699.
[20] Y. Ozaki, S. Suzuki, M. Morimitsu, M. Matsunaga, *Sens. Actuators, B* **2000**, *62*, 220.
[21] A. C. Romain, J. Nicolas, *Sens. Actuators, B* **2010**, *146*, 502.
[22] U. Lommatzsch, J. Ihde, *Plasma Processes Polym.* **2009**, *6*, 642.
[23] D. Kathiravan, B.-R. Huang, *J. Mater. Chem. C* **2018**, *6*, 2387.
[24] O. Lupan, S. Shishiyanu, L. Chow, T. Shishiyanu, *Thin Solid Films* **2008**, *516*, 3338.
[25] V. Postica, M. Hoppe, J. Gröttrup, P. Hayes, V. Röbisch, D. Smazna, R. Adelung, B. Viana, P. Aschehoug, T. Pauporté, O. Lupan, *Solid State Sci.* **2017**, *71*, 75.
[26] V. Postica, A. Vahl, D. Santos-Carballal, T. Dankwort, L. Kienle, M. Hoppe, A. Cadi-Essadek, N. H. de Leeuw, M.-I. Terasa, R. Adelung, F. Faupel, O. Lupan, *ACS Appl. Mater. Interfaces* **2019**, *11*, 31452.
[27] V. Postica, A. Vahl, J. Strobel, D. Santos-Carballal, O. Lupan, A. Cadi-Essadek, N. H. de Leeuw, F. Schütt, O. Polonskyi, T. Strunskus, M. Baum, L. Kienle, R. Adelung, F. Faupel, *J. Mater. Chem. A* **2018**, *6*, 23669.
[28] N. Ababii, M. Hoppe, S. Shree, A. Vahl, M. Ulfa, T. Pauporté, B. Viana, V. Cretu, N. Magariu, V. Postica, V. Sontea, M.-I. Terasa, O. Polonskyi, F. Faupel, R. Adelung, O. Lupan, *Sens. Actuators, A* **2019**, *293*, 242.
[29] L. Chow, O. Lupan, G. Chai, H. Khallaf, L. K. Ono, B. R. Cuenya, I. M. Tiginyanu, V. V. Ursaki, V. Sontea, A. Schulte, *Sens. Actuators, A* **2013**, *189*, 399.
[30] J. F. Moulder, W. F. Stickle, P. E. Sobol, K. D. Bomben, *Handbook of X-ray Photoelectron Spectroscopy: A Reference Book of Standard Spectra for Identification and Interpretation of XPS Data*, PerkinElmer, Eden Prairie, MN, USA **1992**.
[31] C. D. Wagner, A. V. Naumkin, A. Kraut-Vass, J. W. Allison, C. J. Powell, J. R. Rumble Jr., *NIST Standard Reference Database 20*, Version 3.2 (Web Version).
[32] Y. Natsume, H. Sakata, *Thin Solid Films* **2000**, *372*, 30.
[33] Y. Natsume, H. Sakata, T. Hirayama, *Phys. Status Solidi A* **1995**, *148*, 485.
[34] Y. Zhang, K. Yu, D. Jiang, Z. Zhu, H. Geng, L. Luo, *Appl. Surf. Sci.* **2005**, *242*, 212.
[35] J. Fan, R. Freer, *J. Appl. Phys.* **1995**, *77*, 4795.
[36] S.-T. Kuo, W.-H. Tuan, J. Shieh, S.-F. Wang, *J. Eur. Ceram. Soc.* **2007**, *27*, 4521.
[37] J. D. Choi, G. M. Choi, *Sens. Actuators, B* **2000**, *69*, 120.
[38] F. A. Kröger, H. J. Vink, in *Solid State Physics*, Vol. *3* (Eds: F. Seitz, D. Turnbull), Academic Press, Cambridge, MA **1956**, p. 307.
[39] S. Y. Li, P. Lin, C. Y. Lee, T. Y. Tseng, C. J. Huang, *J. Phys. D: Appl. Phys.* **2004**, *37*, 2274.
[40] S. Venkataraj, S. Hishita, Y. Adachi, I. Sakaguchi, K. Matsumoto, N. Saito, H. Haneda, N. Ohashi, *J. Electrochem. Soc.* **2009**, *156*, H424.
[41] F. J. Sheini, D. S. Joag, M. A. More, *Thin Solid Films* **2010**, *519*, 184.
[42] O. Lupan, V. Cretu, V. Postica, M. Ahmadi, B. R. Cuenya, L. Chow, I. Tiginyanu, B. Viana, T. Pauporté, R. Adelung, *Sens. Actuators, B* **2016**, *223*, 893.
[43] C. Soci, A. Zhang, B. Xiang, S. A. Dayeh, D. P. R. Aplin, J. Park, X. Y. Bao, Y. H. Lo, D. Wang, *Nano Lett.* **2007**, *7*, 1003.
[44] V. Postica, I. Paulowicz, O. Lupan, F. Schütt, N. Wolff, A. Cojocaru, Y. K. Mishra, L. Kienle, R. Adelung, *Vacuum* **2019**, *166*, 393.
[45] L. Hromádko, E. Koudelková, R. Bulánek, J. M. Macak, *ACS Omega* **2017**, *2*, 5052.
[46] A. V. Bandura, J. D. Kubicki, J. O. Sofo, *J. Phys. Chem. C* **2011**, *115*, 5756.
[47] V. Mankad, P. K. Jha, *AIP Adv.* **2016**, *6*, 085001.
[48] G. Cicero, J. C. Grossman, A. Catellani, G. Galli, *J. Am. Chem. Soc.* **2005**, *127*, 6830.
[49] A. Vahl, O. Lupan, D. Santos-Carballal, V. Postica, S. Hansen, H. Cavers, N. Wolff, M.-I. Terasa, M. Hoppe, A. Cadi-Essadek, T. Dankwort, L. Kienle, N. H. de Leeuw, R. Adelung, F. Faupel, *J. Mater. Chem. A* **2020**, *8*, 16246.
[50] M. W. Ahn, K. S. Park, J. H. Heo, J. G. Park, D. W. Kim, K. J. Choi, J. H. Lee, S. H. Hong, *Appl. Phys. Lett.* **2008**, *93*, 263103.
[51] X. Wang, P. Ren, H. Tian, H. Fan, C. Cai, W. Liu, *J. Alloys Compd.* **2016**, *669*, 29.
[52] O. Bikondoa, C. L. Pang, R. Ithnin, C. A. Muryn, H. Onishi, G. Thornton, *Nat. Mater.* **2006**, *5*, 189.
[53] R. Schaub, P. Thostrup, N. Lopez, E. Lægsgaard, I. Stensgaard, J. K. Nørskov, F. Besenbacher, *Phys. Rev. Lett.* **2001**, *87*, 266104.
[54] M. Gong, Y. Li, Y. Guo, X. Lv, X. Dou, *Sens. Actuators, B* **2018**, *262*, 350.
[55] O. Lupan, L. Chow, T. Pauporté, L. K. Ono, B. Roldan Cuenya, G. Chai, *Sens. Actuators, B* **2012**, *173*, 772.
[56] V. Postica, F. Schütt, R. Adelung, O. Lupan, *Adv. Mater. Interfaces* **2017**, *4*, 1700507.
[57] O. Lupan, V. Postica, F. Labat, I. Ciofini, T. Pauporté, R. Adelung, *Sens. Actuators, B* **2018**, *254*, 1259.
[58] O. Lupan, V. Postica, J. Gröttrup, A. K. Mishra, N. H. de Leeuw, R. Adelung, *Sens. Actuators, B* **2017**, *245*, 448.
[59] C. Lupan, R. Khaledialidusti, A. K. Mishra, V. Postica, M.-I. Terasa, N. Magariu, T. Pauporté, B. Viana, J. Drewes, A. Vahl, F. Faupel, R. Adelung, *ACS Appl. Mater. Interfaces* **2020**, *12*, 24951.
[60] O. Lupan, V. Postica, J. Gröttrup, A. K. Mishra, N. H. de Leeuw, J. F. C. Carreira, J. Rodrigues, N. Ben Sedrine, M. R. Correia, T. Monteiro, V. Cretu, I. Tiginyanu, D. Smazna, Y. K. Mishra, R. Adelung, *ACS Appl. Mater. Interfaces* **2017**, *9*, 4084.
[61] V. Postica, J. Gröttrup, R. Adelung, O. Lupan, A. K. Mishra, N. H. de Leeuw, N. Ababii, J. F. C. Carreira, J. Rodrigues, N. B. Sedrine, M. R. Correia, T. Monteiro, V. Sontea, Y. K. Mishra, *Adv. Funct. Mater.* **2017**, *27*, 1604676.
[62] M. Nyberg, M. A. Nygren, L. G. M. Pettersson, D. H. Gay, A. L. Rohl, *J. Phys. Chem.* **1996**, *100*, 9054.
[63] T. Krüger, L. Hansen, H. Kersten, *J. Phys.: Conf. Ser.* **2020**, *1492*, 012023.
[64] S. Daria, S. Sindu, H. Mathias, H. Luka, M. Janik, D. Jannes, K. Zaho, F. Bodo, K. Holger, A. Rainer, *Contrib. Plasma Phys.* **2018**, *58*, 384.

[65] C. Merten, C. Regula, A. Hartwig, J. Ihde, R. Wilken, *Plasma Processes Polym.* **2013**, *10*, 60.
[66] Y. A. Ussenov, L. Hansen, T. Krüger, T. S. Ramazanov, H. Kersten, *Jpn. J. Appl. Phys.* **2020**, *59*, SHHE06.
[67] V. Cretu, V. Postica, A. K. Mishra, M. Hoppe, I. Tiginyanu, Y. K. Mishra, L. Chow, N. H. de Leeuw, R. Adelung, O. Lupan, *J. Mater. Chem. A* **2016**, *4*, 6527.
[68] O. Lupan, V. Cretu, V. Postica, O. Polonskyi, N. Ababii, F. Schütt, V. Kaidas, F. Faupel, R. Adelung, *Sens. Actuators, B* **2016**, *230*, 832.
[69] H. T. Hsueh, T. J. Hsueh, S. J. Chang, F. Y. Hung, T. Y. Tsai, W. Y. Weng, C. L. Hsu, B. T. Dai, *Sens. Actuators, B* **2011**, *156*, 906.
[70] D. Gedamu, I. Paulowicz, S. Kaps, O. Lupan, S. Wille, G. Haidarschin, Y. K. Mishra, R. Adelung, *Adv. Mater.* **2014**, *26*, 1541.